Geophysical Research Letters

Key Points:

- The 11-year solar cycle produces a footprint in Northeastern Pacific sea surface temperatures (SSTs) that modulate variations in the Pacific meridional mode
- The solar influence is first amplified in the stratosphere and then alters the Hadley circulation to induce the SST footprint in NE Pacific
- The SST footprint modulates El Niño-Southern Oscillation (ENSO) activities, resulting in more central Pacific (CP) El Niño (La Niña) events during the active (inactive) solar phase

Correspondence to:

J.-Y. Yu,
jyyu@uci.edu

The Footprint of the 11-Year Solar Cycle in Northeastern Pacific SSTs and Its Influence on the Central Pacific El Niño

Yong-Fu Lin[1] , **Jin-Yi Yu[1]** , **Chau-Ron Wu[2]** , and **Fei Zheng[3]**

[1]Department of Earth System Science, University of California, Irvine, CA, USA, [2]Department of Earth Sciences, National Taiwan Normal University, Taipei, Taiwan, [3]International Center for Climate and Environment Science (ICCES), Institute of Atmospheric Physics, Chinese Academy of Sciences, Beijing, China

Abstract Applying statistical analyses to reanalysis products during the period 1900–2018, this study finds the 11-year solar cycle to have a significant correlation with sea surface temperature (SST) variations in the Northeastern Pacific. The solar influence is first manifested and amplified in the lower stratosphere, which then alters the strength of Hadley circulation in the troposphere. Lastly, the changes in the sinking branch of the Hadley circulation modulate surface heat fluxes to give rise to the SST footprint. The footprint has a structure similar to that of the Pacific meridional mode (PMM) that is known to be an important trigger of the central Pacific (CP) type of the El Niño-Southern Oscillation (ENSO). The 11-year solar cycle is thus shown to contribute to the slow modulation of the CP ENSO and, in particular, to be associated with more CP El Niño (La Niña) events during the active (inactive) phase of the cycle.

Plain Language Summary Sun spot activity is known to exhibit increase and decrease in a regular cycle that lasts about 11 years. This 11-year solar cycle modulates the amount of solar radiation emitted by the Sun and received by the earth's climate system. In this study, we show that this solar cycle can induce a ~0.2°C sea surface temperature (SST) variation in the Northeastern Pacific. Statistical analyses are performed to show that the influence of the solar cycle is first amplified in the lower stratosphere and then descends to influence the strength of the Hadley circulation in the troposphere. The change in the Hadley circulation then results in the SST footprint in the Northeastern Pacific via surface heat fluxes. The SST variations can then extend into the tropical Pacific to modulate the occurrence frequencies of a particular type of El Niño and La Niña event in the central Pacific (CP). It is found that more CP El Niño events occur during the active phase of the solar cycle, while more CP La Niña events occur during the inactive phase.

1. Introduction

Sunspot activity waxes and wanes on a cycle with a period of 11 years (Braun et al., 2005; Hathaway, 2015). This 11-year solar cycle modulates the amount of irradiance impinging on the earth's climate system. Past studies have found evidence that the solar cycle may induce significant climate variability in the atmosphere and oceans. 11-year signals or modulation effects, for example, have been found in the stratospheric temperature, ozone concentration, and meridional circulation (e.g., Kodera & Kuroda, 2002; Shindell et al., 2020). In the troposphere, solar cycle signals have been found in jetstream variations related to the northern and southern annular modes (e.g., Kuroda, 2018; Kuroda & Kodera, 2005; Lee & Hameed, 2007; Lee et al., 2008), surface pressure variations related to the North Atlantic Oscillation (e.g., Chiodo et al., 2019; Gray et al., 2016; Thiéblemont et al., 2015), sea surface temperature variations in the eastern tropical Pacific, and precipitation maximum in the tropical Pacific (Meehl & Arblaster, 2009; Meehl et al., 2008, 2009; Misios et al., 2019; Roy, 2014; Van Loon et al., 2007).

However, the changes in solar irradiance associated with the solar cycle amount to only about 0.1% of the total solar irradiance (TSI) reaching the top of earth's atmosphere (Lean et al., 2005). How can this small variation in solar radiation leave measurable footprints in earth's climate? Efforts had been made to identify mechanisms that can amplify the small radiation variations so that they become large enough to impact the climate. At least two mechanisms have been suggested: one is a "top-down" mechanism that invokes radiation-circulation interactions in the stratosphere and the other is a "bottom-up" mechanism that

invokes air-sea interactions at the ocean surface. In the "top-down" mechanism, the small radiative forcing variations associated with the solar cycle induce a significant change in the residual meridional circulation of the stratosphere. The circulation change amplifies the solar cycle forcing to impact the climate system (Andrews et al., 2015; Gray et al., 2010; Kodera & Kuroda, 2002; Kodera et al., 2016). In the "bottom-up" mechanism, the initial solar effect on ocean sea surface temperatures (SSTs) can be amplified via positive air-sea feedbacks among surface winds and evaporation, convective precipitation, and upper ocean dynamic processes (Meehl & Arblaster, 2009; Meehl et al., 2008, 2009; Gray et al., 2010).

Although the radiative forcing from the solar cycle is uniform at the top of the atmosphere, its climate impacts can vary geographically due to geographical variations in the amplification mechanisms. For example, the "top-down" mechanism converts the direct solar radiative effect into an indirect dynamical effect related to subtropical jet displacement and changes in the Brewer-Dobson circulation. As pointed out by Kodera and Kuroda (2002), the former process has a greater impact on middle and high latitudes, while the latter process can also impact tropical regions. This amplification mechanism therefore may induce different solar cycle impacts for different latitudinal regions. Similarly, the "bottom-up" mechanism was suggested to work most effectively over the clear-sky regions of the tropical and subtropical oceans where the solar radiation changes associated with the solar cycle can impact SSTs (Meehl et al., 2008). In these regions, the variations in irradiance at the surface associated with the solar cycle forcing can be one order of magnitude greater than the globally averaged values. These are also regions where the atmosphere and oceans are strongly coupled. This geographical dependence of the amplification mechanism may cause the 11-year solar cycle to leave stronger footprints in certain regions.

In this study, we conduct statistical analyses with observations and reanalysis products and find that the 11-year solar cycle leaves the strongest SST footprint in the Northeastern (NE) Pacific. Both the "top-down" and "bottom-up" mechanisms are used to explain this geographic preference of the solar cycle impacts. We further notice that the footprint resembles the most prominent SST variability in the region, known as the Pacific Meridional Mode (PMM; Chiang & Vimont, 2004). Given the close linkage between the PMM and El Niño-Southern Oscillation (ENSO) events, we investigate further the links between the solar cycle and ENSO and show that the 11-year solar cycle can modulate the activities of a particular type of ENSO event named the Central Pacific (CP) ENSO (Kao & Yu, 2009; Yu & Kao, 2007).

2. Data and Methods

The monthly SSTs used are from the Extended Reconstructed Sea Surface Temperature (ERSST) version 5 provided by the National Centers for Environmental Information/National Oceanic and Atmospheric Administration (Huang et al., 2017). The data set has a 2° × 2° horizontal resolution and is available from 1854 to the present. Monthly atmospheric variables (such as wind fields, surface heat fluxes, and total cloud cover) were from the National Centers for Environmental Prediction/National Center for Atmospheric Research (NCEP/NCAR) reanalysis 1 (Kalnay et al., 1996). The data set has a 1.875° × 1.875° horizontal resolution and is available from year 1948 to the present. Anomalies are defined as the deviations from the monthly climatology calculated from the respective analysis periods (either 1948–2018 or 1900–2018) after removing their linear trends.

We use the sunspot number (SSN) totaled throughout a calendar year to represent solar cycle (SC) variations. The SSN data were obtained from the World Data Center SILSO, Royal Observatory of Belgium, Brussels. We considered times during which the value of SSN exceeded 100 as an active period and less than 20 as an inactive period (Ratnam et al., 2014). Monthly values of the TSI during 1900–2018 were estimated by Kopp et al. (2016) using Community-Consensus TSI Composite and models and obtained from Gregg Kopp's TSI Page, University of Colorado. This data set is believed to be the most realistic and upto-date estimate of the solar variability over the last 400 years (Kopp et al., 2016).

A CP index was used to represent the intensity of the CP ENSO. This index was calculated using the regression-empirical orthogonal function (EOF) analysis method of Kao & Yu (2009). In this method, the SST anomalies regressed onto the Niño1+2 SST index (0–10°S; 80°W–90°W) are removed from the total SST anomalies before an EOF analysis was applied to obtain the spatial pattern of the CP ENSO (i.e., the leading EOF pattern). The principal component of the leading EOF mode is defined as the CP index. Follow previous studies (Ding et al., 2017; Paek et al., 2017; Yu & Kim, 2013), this procedure identifies a total of 16 CP El Niño and 19 CP La Niña events during 1900–2016 (also see Table S1).

A PMM index was used to represent the intensity of PMM. This index is defined as the SST expansion coefficient from a Maximum Covariance Analysis (MCA) when it is applied to combined SST and surface wind anomalies over a subtropical Pacific region (21°S–32°N and 175°E−95°W; Chiang & Vimont, 2004). The linear trend and the regression onto an equatorial Pacific Cold Tongue Index (SST averaged over 180–90°W, 6°S–6°N) were removed from the anomalies before the analysis.

A sea level pressure (SLP) index is used to represent the intensity of the North Pacific Oscillation (NPO). Followed Guo and Sun (2004), the NPO index is calculated as the difference between SLP anomalies averaged in a North Pacific region (50°–65°N, 130°–170°W) and SLP anomalies averaged in a subtropical Pacific region (25°–40°N, 130°E−170°W).

The statistical significance of the results was examined at the 90% and 95% levels. In the significance tests, the effective degree of freedom was determined using an auto-correlation method.

3. Results

3.1. An SST Footprint of the 11-Year Solar Cycle in the Northeastern Pacific

Figure 1a shows the variations in the annual SSN from 1900 to 2018. The variations are clearly dominated by an 11-year cycle. The cycle amplitude varies, showing an increasing trend from 1900 to 1965 and a decreasing trend from 1965 to present. The corresponding changes in irradiance are small, as the TSI value varies from ∼1,360 W/m^2 during inactive phases of the solar cycle to ∼1,362 W/m^2 during active phases. Here we use the TSI to represent the amplitude of the 11-year cycle, but it should be noted that for stratospheric dynamics where the solar cycle has a strong interaction with the atmosphere what matters most is spectral solar irradiance (Matthes et al., 2017). Since the NCAR/NCEP Reanalysis 1 atmospheric data set covers only the period 1948–2019, we focus on this period to examine the solar footprint and associated physical mechanisms. As shown in Figure 1a, this period includes six solar cycles. We regressed global SST anomalies onto the annual SSN value during 1948–2018 to examine the solar footprint in SSTs. Figures 1b and 1c show the regressions between the annual SSN and the summer and winter half-years of the SST anomalies. Following Seager et al. (2005), the summer half-year is from June to November (JJASON, hereafter) and the winter half-year is from December to the following May (DJFMAM, hereafter). The regression patterns are similar during the two seasons, but the magnitudes are stronger in winter than in summer. The strongest and most significant regressions appear in the NE Pacific and around the Antarctic. The solar cycle is associated with warm SST anomalies in these two regions during its active phase and cold SST anomalies during its inactive phase. Similar patterns were found in the composite SST differences between the active and inactive periods of the solar cycle for the two seasons (Figures 1d and 1e). The composite analysis reveals that the solar footprints in SSTs are about 0.2°C in magnitude. We repeated the analyses with the longer SSN and SST datasets covering the entire period (1900–2018) and obtained similar solar footprints (Figure S1). Similar SST footprints are obtained when repeating the analyses with 7-year low-pass filtered SST anomalies (Figure S2). This similarity indicates that the solar influences operate primarily on decadal timescales.

In this study, we focus on understanding the solar footprint in the NE Pacific SSTs due to their importance to the development of CP ENSO events. We are interested in learning how the spatially uniform solar cycle forcing in solar irradiance can give rise to this localized SST footprint and whether the solar cycle can influence ENSO activities.

We first examine how atmospheric temperatures respond to the solar cycle forcing. We regress in Figure 2a the winter (DJFMAM) anomalies in zonal-mean air temperature onto the yearly SSN during the analysis period. The figure shows that the solar cycle forcing induces widespread warming in the middle and upper atmosphere (above 200 hPa), which is expected from absorption by ozone of the increased ultraviolet radiation. The warming is particularly large in the middle-to-lower stratosphere (with an amplitude close to 0.2°C), where the maximum ozone concentration resides. This is consistent with previous studies (e.g., Frame & Gray, 2010; Hood & Soukharev, 2012; Kodera & Kuroda, 2002; Mitchell et al., 2015; Shindell et al., 2020), as those also show warming in the lower stratosphere of about 0.2°C–0.5°C associated with the solar cycle. The stratospheric amplification mechanism (e.g., Kodera & Kuroda, 2002) explains this stratospheric warming in the following way. The solar cycle heating first changes the equator-to-pole tempera-
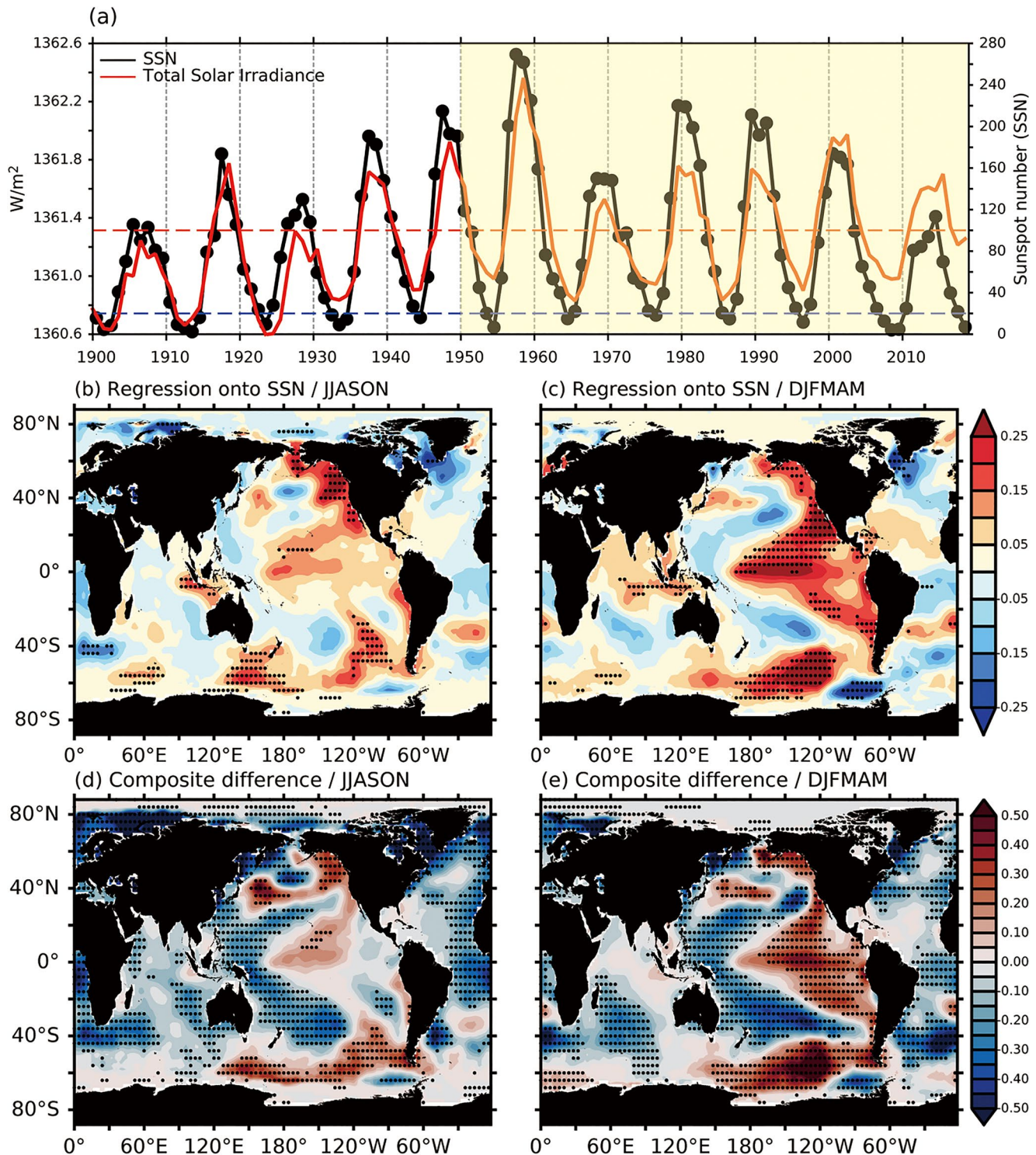
Figure 1. (a) Yearly time series of sunspot number (SSN, red line) and total solar irradiance (TSI, black line). The red and blue dashed lines indicate the thresholds used to define active (SSN≥100) and inactive (SSN≤20) periods, respectively. (b) Regression of JJASON SST anomalies onto the yearly SSN (unit in °C/100*SSN) at 0 year lag during 1948–2018 (yellow colored periods in Figure 1a). (c) Same as (b) but for DJFMAM. (d) The difference of composite JJASON SST anomalies (⁰C) between solar active and inactive periods during 1948–2018 (yellow colored periods in Figure 1a). (e) Same as (d) but for DJFMAM. The stippled areas (in b–e) indicate significance at the 95% confidence level determined using a Student's *t*-test. DJFMAM, December to May; JJASON, June to November; SST, sea surface temperature.
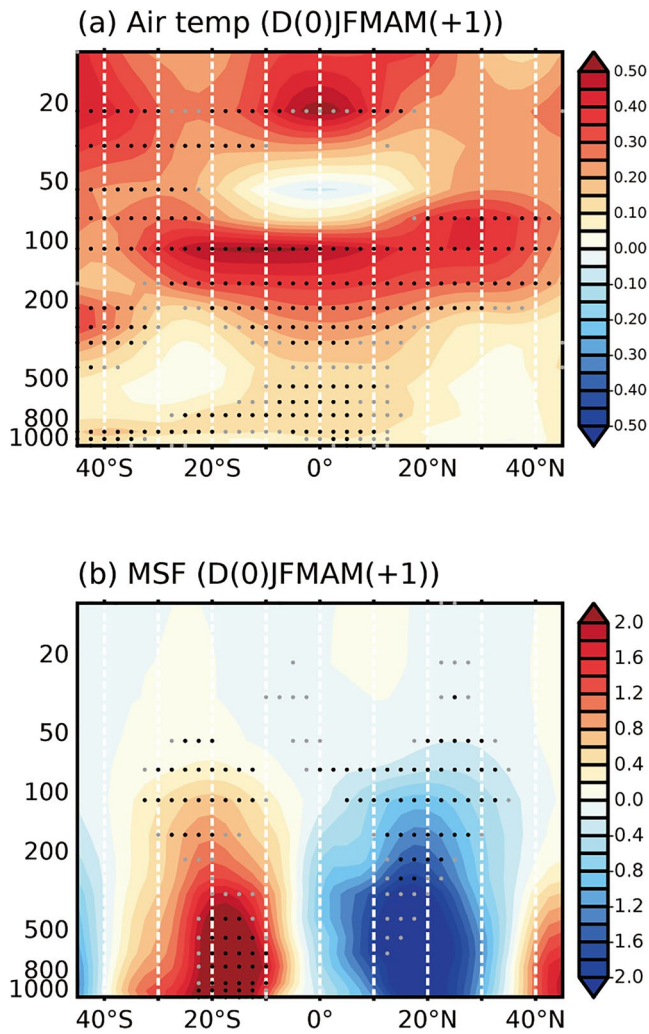
(a) Air temp (D(0)JFMAM(+1))

(b) MSF (D(0)JFMAM(+1))

Figure 2. Regressions of DJFMAM zonal-mean global air temperature (a, °C/100 × SSN) and NEP (180°W–100°W) mass streamfunction profile (b, 10^{11} kg/s/100 × SSN) onto the yearly SSN during 1948–2018. Positive (negative) values indicate clockwise circulations (counter-clockwise) in (b). Gray (black) stippled areas indicate significance at the 90% (95%) confidence level determined using a Student's *t*-test. DJFMAM, December to May; NEP, Northeastern Pacific, SSN, sunspot number.

ture gradient, which then affects the strength of the polar stratospheric jet and the path of upward propagating planetary waves. These waves deposit their zonal momentum on the poleward side of the jet, weakening the Brewer-Dobson circulation (BDC). The reduced upwelling rates advectively increase ozone mixing ratios, leading to warming in the lower stratosphere during the active phase of the solar cycle.

In the tropics, the anomalous descent associated with the weakened BDC extends the lower stratospheric warming into the upper troposphere. It is possible that the upper troposphere warming increases the stability of the troposphere and then causes the Hadley cell (HC) to weaken. During boreal winter, it is known that the HC is dominated by its winter branch into the northern hemisphere (Lindzen & Hou, 1988). Since the northern hemispheric branch has its sinking branch over the NE Pacific, the solar cycle forcing might induce SST variations (i.e., the SST footprint) in the NE Pacific. To examine this possibility, we show in Figure 2b the anomalous HC induced by the solar cycle. The anomalous HC is obtained by regressing the DJFMAM mass streamfunction averaged over the longitudinal sector of the NE Pacific (180°W–100°W) onto the yearly SSN. The positive (negative) values in Figure 2b indicate a clockwise (counter-clockwise) circulation. Figure 2b confirms that during winter the HC weakens significantly during the active phase of the solar cycle. The summer branch (into the southern hemisphere) also weakens but not as much. We find a negative correlation coefficient (−0.46, $P < 0.1$) between the yearly SSN and a NE Pacific HC index. The NE Pacific HC index is defined as the mass streamfunction averaged over a Pacific region between 0°N–30°N and 180°W–100°W (cf. Wang, 2002). The NE Pacific HC index was low-pass filtered using a 5-year running mean after removing its linear trends. The result of this correlation analysis indicates that the solar cycle can weaken (strengthen) the NE Pacific-sector HC during its active (inactive) phase by increasing (decreasing) the stability of the troposphere.

We next examine the regressions between the yearly SSN and DJFMAM anomalies of key atmospheric and oceanic variables over the North Pacific. The regression with SST anomalies (Figure 3a) reproduces the NE Pacific footprint of the solar cycle (cf. Figure 1c). The SST footprint is accompanied by a negative SLP anomaly and anomalous cyclonic circulation off northwestern North America (Figure 3b). This anomalous SLP center reflects a weakening of the Pacific subtropical high due to the weakened HC. The weakened subtropical high can lead to a reduction in total cloud cover in the region (Figure 3c). This is because the clouds in the NE Pacific is mostly stratus clouds and the descending motions

associated with the sinking branch of the HC are a key factor in the formation of marine stratus clouds (e.g., Klein & Hartmann, 1993). Therefore, a weakened HC and resulting weaker descending motions can decrease the cloudiness (i.e., marine boundary clouds) in the NE Pacific. While the decreased cloudiness allows more shortwave radiation flux (Figure 3e) to reach the surface and increase the NE Pacific SSTs, some of this heating effect is canceled out by the cooling caused by increased upward longwave radiative flux at the surface (Figure 3f). In Figure 3, the surface flux is defined positive downward (i.e., heating ocean surface) and negative upward (i.e., cooling ocean surface). At the same time, the anomalous cyclonic circulation weakens subtropical trade winds, reducing latent and sensible heat fluxes (i.e., heating effects) off the North American coast (Figures 3g and 3h). The net heat flux anomaly (Figure 3d) has positive values (i.e., a heating effect) off the North American coast. The surface warming induced there (cf. Figure 3a) can be spread southwestward toward the equatorial Pacific via subtropical Pacific coupled processes (e.g., Vimont et al., 2003; Xie & Philander, 1994; Yu & Fang, 2018). Combining the HC-induced thermodynamical processes and the subtropical Pacific coupling, we are able to explain how the active (inactive) phase of the so-
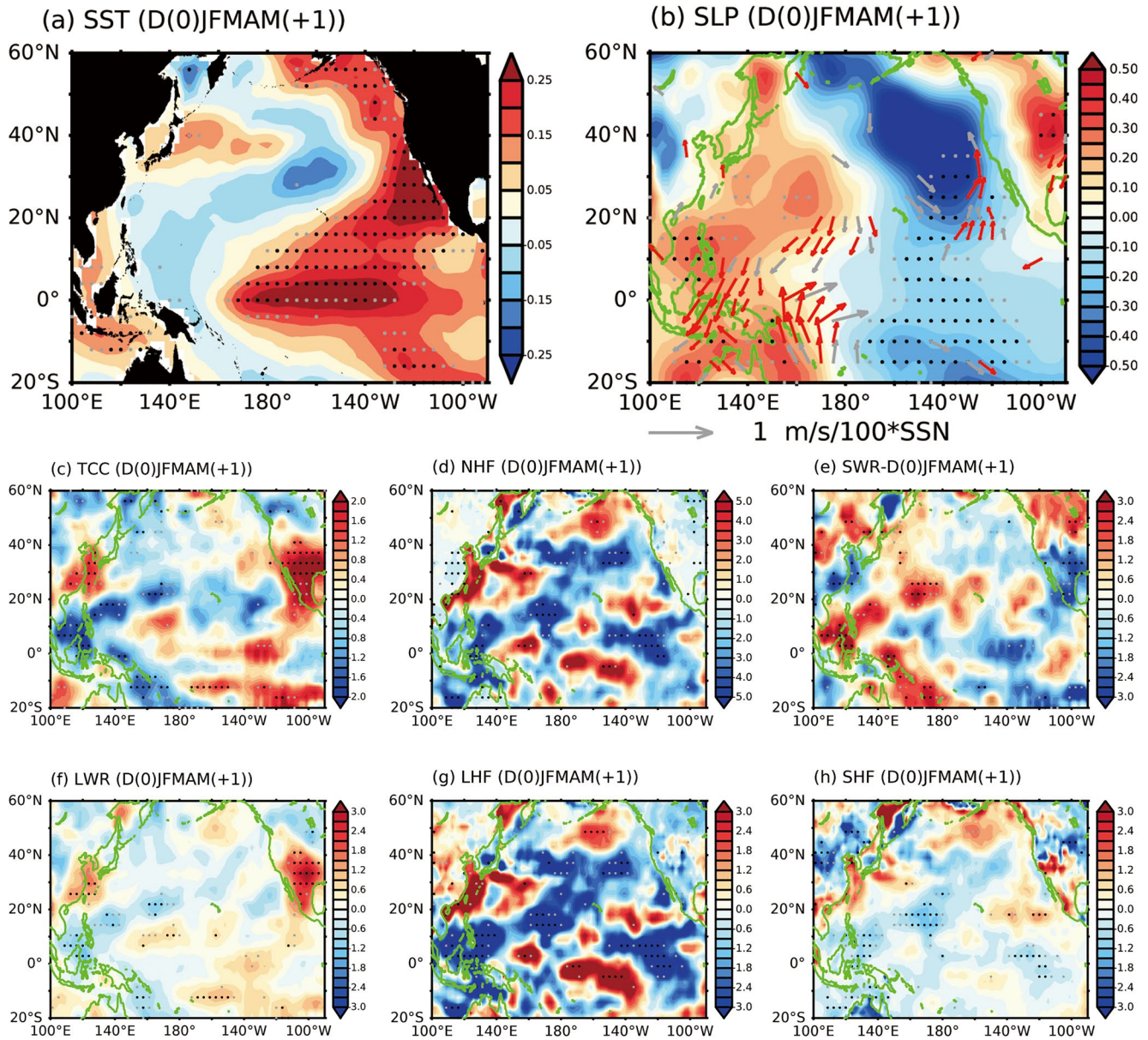
Figure 3. Regressions onto the yearly SSN during 1948–2018 of DJFMAM anomalies in SST (°C/100 *SSN) (a), SLP (color, hPa/100*SSN) and 1000 hPa wind (arrows) (b), total cloud cover (%/100*SSN) (c), net heat flux anomalies (W/m^2/100*SSN) (d), shortwave radiation (W/m^2/100*SSN) (e), longwave radiation (W/m^2/100*SSN) (f), latent heat flux (W/m^2/100*SSN) (g), and sensible heat flux (W/m^2/100*SSN) (h). Positive values in (d)–(h) indicate fluxes from the atmosphere to the ocean and vice versa for negative values. Gray (black) stippled areas and gray (red) vectors (in b) indicate significance at the 90% (95%) confidence level determined using a Student's *t*-test. DJFMAM, December to May; SLP, sea level pressure; SSN, sunspot number.

lar cycle can induce a warm (cold) SST footprint extending southwestward from the North American coast toward the tropical central Pacific. It should be noted that after the warm (cold) SST anomalies arrive in the central tropical Pacific, they can further excite an atmospheric wave train that propagates into midlatitudes to further weakens (strengthens) the subtropical high in the NE Pacific (Lyu and Yu et al., 2017).

3.2. Solar Cycle Modulation of PMM and ENSO Activities

It is interesting to note that the solar footprint in the NE Pacific SSTs closely resembles the SST anomaly pattern associated with the PMM. Similar patterns were obtained when we regress DJFMAM Pacific SSTAs onto the DJFMAM PMM index (Figure S3a) and yearly SSN (Figure 3a). Their pattern correlation coefficient is as high as 0.6 (*P* < 0.01). We also compared the regressed SLP, wind, and net surface flux patterns

with the PMM, yearly SSN, and the HC index (Figure S3) and found them to be very similar. Our analyses suggest that, through the HC mechanism, the 11-year solar cycle has an SST footprint in the NE Pacific that projects strongly onto the PMM pattern. Since the PMM is known to be a key trigger of the CP type of ENSO event (Kim et al., 2012; Lin et al., 2015; Yu et al., 2010, 2012, 2015; see Yu et al., 2017 for a review), this correlation implies that the solar cycle may play some role in modulating CP ENSO activity. El Niño events may occur more frequently during the active phase of the solar cycle, while CP La Niña events may occur more frequently during the inactive phase. Sun and Yu (2009) noticed that ENSO showed a 10–15 years modulation cycle characterized by alternations between a regime with more CP El Niño events and a regime with more CP La Niña events. Pascolini-Campbell et al. (2015) used nine different methods and five SST datasets to distinguish between the CP El Niño and the canonical El Niño. They also pointed out that the role of multidecadal natural climate variability is important in the generation of CP El Niños. The 11-year solar cycle may be a contributing factor to this modulation cycle. Also, it is interesting to note that the Yu et al. (2012) argued that the CP ENSO events are more closely associated with HC variations, while the conventional Eastern Pacific (EP) ENSO events are more closely associated with variations in the Walker circulation.

We examine in Figure 4a the relationships of the yearly SSN value to the DJFMAM values of the PMM and CP indices during 1948–2018. It should be noted that the PMM is strongest during boreal winter and spring (Chiang & Vimont, 2004), while the CP ENSO peaks during boreal winter (Kao & Yu, 2009). The figure indicates that there is a tendency for these three indices to co-vary on decadal timescales. The values of the PMM and CP indices tend to have their maximum values close to the peak in the active phase of the solar cycle and their minimum values close to the nadir of the inactive phase. Figure 4b shows that the PMM index has its largest correlation with the SSN at lag 0, while the CP index has its largest correlation with the SSN at a one-year lag. These lagged correlations imply that the solar cycle, in its active phase, can strengthen the PMM in the same year and be followed by enhanced CP El Niño activity during the following winter, and vice versa for the inactive phase of the solar cycle. The one-year lag is consistent with the known fact that the PMM in one winter can trigger a CP ENSO to develop and peak during the following winter (e.g., Yu et al., 2017). However, the power spectrum analysis shown in Figures 4c–4e support the influence of the 11-year cycle on the decadal variations of the PMM and CP ENSO. All three indices have a significant peak in power at the 11-year period.

We also counted the numbers of CP El Niño (Paek et al., 2017; Yu & Kim, 2013) and La Niña events (Ding et al., 2017; Yu et al., 2011) during the active and inactive solar phases (i.e., defined as from one year before to one year after the year of the local maximum and minimum SSN values, respectively). In order to have a larger sample size, we performed this analysis for the period 1900–2016. As shown in Figure 4f, 62.5% of the CP El Niño events occurred during the active phase of the solar cycle, but only 37.5% of them occurred during the inactive phase. Conversely, more CP La Niña events occurred during the inactive phase (47.4%) than the active phase (36.8%). This evidence supports the assertion that the 11-year solar cycle is a factor that modulates the occurrence of CP El Niño and La Niña events on decadal timescales.

Previous studies (e.g. Meehl and Arblaster, 2009; Meehl et al., 2008; Misios et al., 2016; van Loon et al., 2007) have suggested that the 11-year solar cycle impacts the Pacific SSTs by first inducing a weak La Niña–like response in the year before the first peak year of the solar cycle and inducing an El Niño-like response 2–3 years later. This sequence is not exactly the same as the one we report here. To explain the difference, we first repeated the composite analysis of Meehl and Arblaster (2009) and van Loon et al. (2007) using the unfiltered SST anomalies. We used the same 12 years selected by Meehl and Arblaster (2009) for the composite (i.e., 1883, 1893, 1905, 1917, 1928, 1937, 1947, 1957, 1968, 1979, 1989, and 2000). We then repeated the composite analysis with high-passed (<7 years) and low-passed (>7 years) filtered SST anomalies. As we show in Figure S4, the "La Niña followed by El Niño" evolution of solar cycle impact appears in the unfiltered and high-pass composites but not in the low-pass composite. This result indicates that the "La Niña followed by El Niño" evolution of solar impact is likely to operate only on interannual timescales. This interannual impact is removed when we regress the SSN onto the original or low-pass filtered SST anomalies (Figure S5). The is due to the fact that the SSN itself has a strong periodic component of about 11 years and its regressions with either the original or low-pass anomalies (i.e., SST and atmospheric variables) are always dominated by the decadal component of the correlations. In summary, the solar cycle impact on Pacific SSTs that we report in this manuscript is a decadal impact that modulates the background SSTs of the Pacific. This decadal impact is different from the interannual impact reported in Meehl and Arblaster (2009)
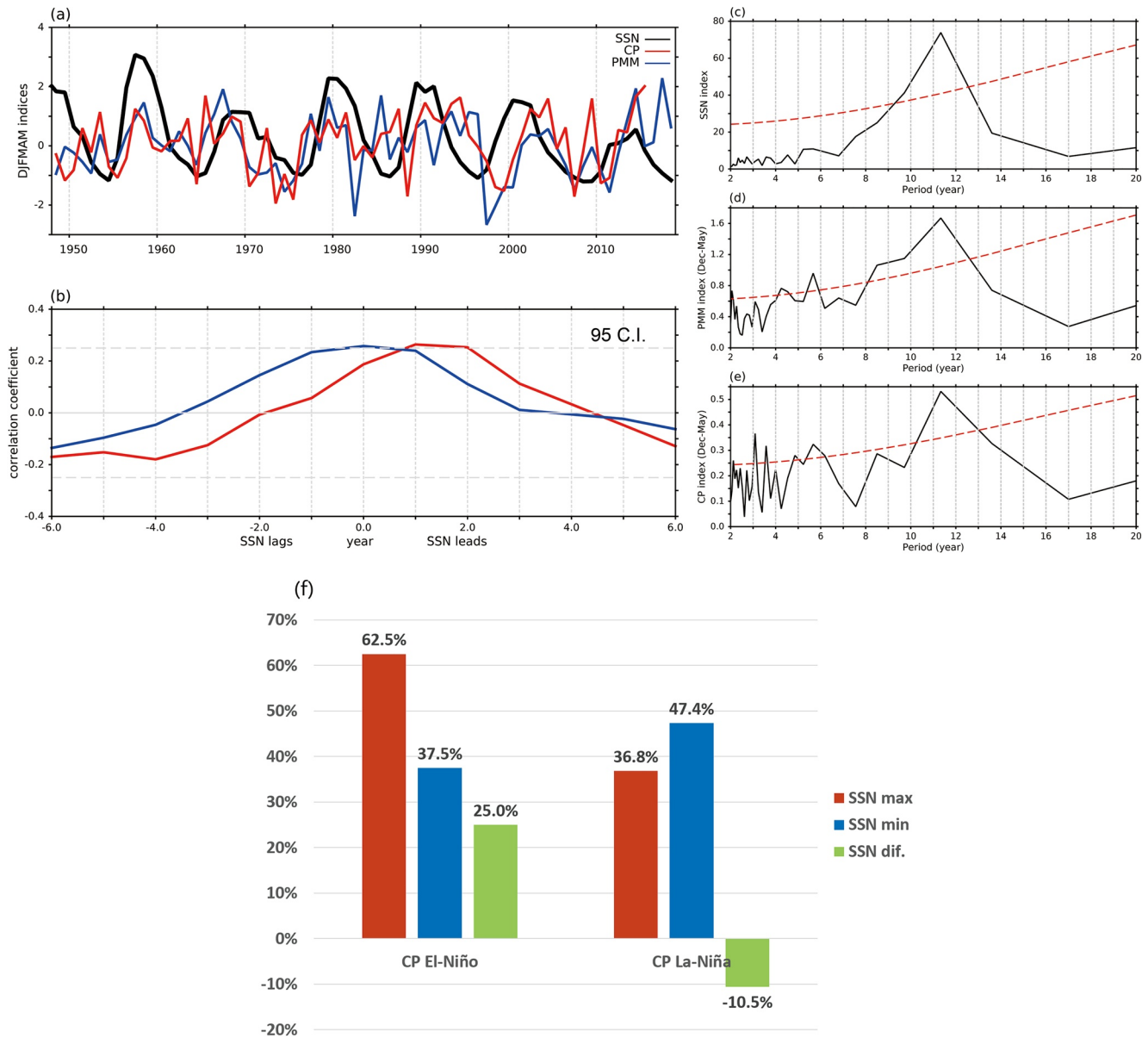
Figure 4. (a) Normalized yearly time series of SSN (black line), DJFMAM CP ENSO (red line), and DJFMAM PMM (blue line) indices. (b) Lag correlation between SSN and DJFMAM CP (red line), DJFMAM PMM (blue line) indices, respectively. Gray dashed lines in (b) indicate significance at the 95% confidence level determined using a Student's *t*-test (c)–(e) Power spectrum for the SSN (c), DJFMAM PMM (d), and DJFMAM CP (e) indices. The dashed lines in (c)–(e) denote the 95% confidence interval against red noise. (f) Percentages of the occurrence of CP El Niño (left bars) and CP La Niña (right bars) events during active solar periods (SSN_{max}, red bars), inactive period (SSN_{min}, blue bars), and their difference (SSN_{max}–SSN_{min}, green bars) during the period 1900–2016. CP, Central Pacific, DJFMAM, December to May; ENSO, El Niño-Southern Oscillation; PMM; Pacific Meridional Mode; SSN, sunspot number.

and van Loon et al. (2007). We emphasize the Hadley circulation and the subtropical Pacific coupling (in the ocean mixed layer) for the decadal impact, while Meehl and Arblaster (2009) emphasized tropical Pacific thermocline dynamics and coupling for the interannual impact.

4. Conclusion and Discussion

This study conducted observational analyses to determine whether a PMM-like SST anomaly in the NE Pacific appears as one of the two strongest SST footprints of the 11-year solar cycle. We showed that, after the small radiative forcing of the solar cycle is amplified via radiative-circulation interactions in the strato-sphere, the solar cycle influence is transmitted to the NE Pacific via the HC. The HC-induced SST variations

in the NE Pacific are then spread to the equatorial Pacific where they modulate the occurrences of CP ENSO events. This modulation is such that CP El Niño events tend to occur more frequently during the active phase of the solar cycle, while CP La Niña events tend to occur more frequently during the inactive phase. These findings imply that the 11-year solar cycle is a relevant source of decadal climate predictability after its small radiative forcing is amplified in the stratosphere and localized to the subtropical Pacific by the Hadley circulation. The active and inactive phases of the 11-year solar cycle have the potential to be used, together with the phase information on the Atlantic Multi-Decadal Oscillation and Pacific Decadal Oscillation, in predicting the occurrence of CP ENSO events (e.g., Kim et al., 2020; Yu et al., 2015).

This study also finds that the other key SST footprint of the solar cycle appears around the Antarctic as a zonal band of SST anomalies. The physical processes that enable the solar cycle to leave this SST footprint were not explored in this study.

Data Availability Statement

The ERSST data were downloaded from the NCEI/NOAA (https://data.nodc.noaa.gov). The NCEP/NCAR Reanalysis 1 data were obtained from their website (https://www.esrl.noaa.gov/psd/data/gridded/data.ncep.reanalysis.html). The yearly SSN is collected by WDCSILSO (http://www.sidc.be/silso/datafiles). The TSI reconstruction data were downloaded from https://spot.colorado.edu/~koppg/TSI/. The CP ENSO and PMM indices were obtained from http://www.aos.wisc.edu/~dvimont/MModes/Data.html and https://www.ess.uci.edu/~yu/2OSC/, respectively.

References

Andrews, M. B., Knight, J. R., & Gray, L. J. (2015). A simulated lagged response of the North Atlantic Oscillation to the solar cycle over the period 1960–2009. *Environmental Research Letters*, *10*(5), 054022. https://doi.org/10.1088/1748-9326/10/5/054022

Braun, H., Christl, M., Rahmstorf, S., Ganopolski, A., Mangini, A., Kubatzki, C., et al. (2005). Possible solar origin of the 1,470-year glacial climate cycle demonstrated in a coupled model. *Nature*, *438*(7065), 208–211. https://doi.org/10.1038/nature04121

Chiang, J. C. H., & Vimont, D. J. (2004). Analogous Pacific and Atlantic meridional modes of tropical atmosphere-ocean variability. *Journal of Climate*, *17*, 4143–4158. https://doi.org/10.1175/JCLI4953.1

Chiodo, G., Oehrlein, J., Polvani, L. M., Fyfe, J. C., & Smith, A. K. (2019). Insignificant influence of the 11-year solar cycle on the North Atlantic Oscillation. *Nature Geoscience*, *12*(2), 94–99. https://doi.org/10.1038/s41561-018-0293-3

Ding, S., Chen, W., Feng, J., & Graf, H. F. (2017). Combined impacts of PDO and two types of La Niña on climate anomalies in Europe. *Journal of Climate*, *30*(9), 3253–3278. https://doi.org/10.1175/JCLI-D-16-0376.1

Frame, T. H. A., & Gray, L. J. (2010). The 11-year solar cycle in ERA-40 data: An update to 2008. *Journal of Climate*, *23*(8), 2213–2222. https://doi.org/10.1175/2009JCLI3150.1

Gray, L. J., Beer, J., Geller, M., Haigh, J. D., Lockwood, M., Matthes, K., et al. (2010). Solar influences on climate. *Reviews of Geophysics*, *48*(4), RG4001. https://doi.org/10.1029/2009RG000282

Gray, L. J., Woollings, T. J., Andrews, M., & Knight, J. (2016). Eleven-year solar cycle signal in the NAO and Atlantic/European blocking. *Quarterly Journal of the Royal Meteorological Society*, *142*(698), 1890–1903. https://doi.org/10.1002/qj.2782

Guo, D., & Sun, Z. B. (2004). Relationships of winter North Pacific Oscillation anomalies with the East Asian winter monsoon and the weather and climate in China. *Journal of Nanjing Institute of Meteorology*, *27*(4), 461–470. https://doi.org/10.1175/JCLI-D-13-00174.1

Hathaway, D. H. (2015). The solar cycle. *Living Reviews in Solar Physics*, *12*(1), 4. https://doi.org/10.1007/lrsp-2015-4

Hood, L. L., & Soukharev, B. E. (2012). The lower-stratospheric response to 11-year solar forcing: Coupling to the troposphere-ocean response. *Journal of the Atmospheric Sciences*, *69*(6), 1841–1864. https://doi.org/10.1175/JAS-D-11-086.1

Huang, B., Thorne, P. W., Banzon, V. F., Boyer, T., Chepurin, G., Lawrimore, J. H., et al. (2017). Extended reconstructed sea surface temperature, version 5 (ERSSTv5): Upgrades, validations, and intercomparisons. *Journal of Climate*, *30*(20), 8179–8205. https://doi.org/10.1175/JCLI-D-16-0836.1

Kalnay, E., Kanamitsu, M., Kistler, R., Collins, W., Deaven, D., Gandin, L., et al. (1996). The NCEP/NCAR 40-year reanalysis project. *Bulletin of the American Meteorological Society*, *77*(3), 437–471. https://doi.org/10.1175/1520-0477(1996)077<0437:TNYRP>2.0.CO;2

Kao, H. Y., & Yu, J. Y. (2009). Contrasting Eastern-Pacific and Central-Pacific types of ENSO. *Journal of Climate*, *22*, 615–632. https://doi.org/10.1175/2008JCLI2309.1

Kim, H. K., Seo, K. H., Yeh, S. W., Kang, N. Y., & Moon, B. K. (2020). Asymmetric impact of Central Pacific ENSO on the reduction of tropical cyclone genesis frequency over the western North Pacific since the late 1990s. *Climate Dynamics*, *54*(1–2), 661–673. https://doi.org/10.1007/s00382-019-05020-8

Kim, S. T., Yu, J. Y., Kumar, A., & Wang, H. (2012). Examination of the two types of ENSO in the NCEP CFS model and its extratropical associations. *Monthly Weather Review*, *140*(6), 1908–1923. https://doi.org/10.1175/MWR-D-11-00300.1

Kodera, K., & Kuroda, Y. (2002). Dynamical response to the solar cycle. *Journal of Geophysical Research*, *107*(D24), 4749. https://doi.org/10.1029/2002JD002224

Kodera, K., Thiéblemont, R., Yukimoto, S., & Matthes, K. (2016). How can we understand the global distribution of the solar cycle signal on the Earth's surface? *Atmospheric Chemistry and Physics*, *16*, 12925–12944. https://doi.org/10.5194/acp-16-12925-2016

Kopp, G., Krivova, N., Wu, C. J., & Lean, J. (2016). The impact of the revised sunspot record on solar irradiance reconstructions. *Solar Physics*, *291*(9–10), 2951–2965. https://doi.org/10.1007/s11207-016-0853-x

Kuroda, Y. (2018). On the origin of the solar cycle modulation of the Southern Annular Mode. *Journal of Geophysical Research: Atmosphere*, *123*(4), 1959–1969. https://doi.org/10.1002/2017JD027091

Kuroda, Y., & Kodera, K. (2005). Solar cycle modulation of the Southern Annular Mode. *Geophysical Research Letters*, *32*(13). https://doi.org/10.1029/2005GL022516

Lean, J., Rottman, G., Harder, J., & Kopp, G. (2005). SORCE contributions to new understanding of global change and solar variability. In *The solar radiation and climate experiment (SORCE)*. (pp. 27–53). New York, NY: Springer.

Lee, J. N., & Hameed, S. (2007). The Northern Hemisphere annular mode in summer: Its physical significance and its relation to solar activity variations. *Journal of Geophysical Research*, *112*, D15111. https://doi.org/10.1029/2007JD008394

Lee, J. N., Hameed, S., & Shindell, D. T. (2008). The northern annular mode in summer and its relation to solar activity variations in the GISS ModelE. *Journal of Atmospheric and Solar-Terrestrial Physics*, *70*(5), 730–741. https://doi.org/10.1016/j.jastp.2007.10.012

Lin, C. Y., Yu, J. Y., & Hsu, H. H. (2015). CMIP5 model simulations of the Pacific meridional mode and its connection to the two types of ENSO. *International Journal of Climatology*, *35*(9), 2352–2358. https://doi.org/10.1002/joc.4130

Lindzen, R. S., & Hou, A. V. (1988). Hadley circulations for zonally averaged heating centered off the Equator. *Journal of the Atmospheric Sciences*, *45*(17), 2416–2427. https://doi.org/10.1175/1520-0469(1988)045<2416:HCFZAH>2.0.CO;2

Lyu, K., Yu, J. Y., & Paek, H. (2017). The influences of the Atlantic multidecadal oscillation on the mean strength of the North Pacific subtropical high during boreal winter. *Journal of Climate*, *30*(1), 411–426. https://doi.org/10.1175/JCLI-D-16-0525.1

Matthes, K., Funke, B., Andersson, M. E., Barnard, L., Beer, J., Charbonneau, P., et al. (2017). Solar forcing for CMIP6 (v3. 2). *Geoscientific Model Development*, *10*(6), 2247–2302. https://doi.org/10.5194/gmd-10-2247-2017

Meehl, G. A., & Arblaster, J. M. (2009). A lagged warm event-like response to peaks in solar forcing in the Pacific region. *Journal of Climate*, *22*(13), 3647–3660. https://doi.org/10.1175/2009JCLI2619.1

Meehl, G. A., Arblaster, J. M., Branstator, G., & Van Loon, H. (2008). A coupled air-sea response mechanism to solar forcing in the Pacific region. *Journal of Climate*, *21*(12), 2883–2897. https://doi.org/10.1175/2007JCLI1776.1

Meehl, G. A., Arblaster, J. M., Matthes, K., Sassi, F., & van Loon, H. (2009). Amplifying the Pacific climate system response to a small 11-year solar cycle forcing. *Science*, *325*(5944), 1114–1118. https://doi.org/10.1126/science.1172872

Misios, S., Gray, L. J., Knudsen, M. F., Karoff, C., Schmidt, H., & Haigh, J. D. (2019). Slowdown of the Walker circulation at solar cycle maximum. *Proceedings of the National Academy of Sciences*, *116*(15), 7186–7191. https://doi.org/10.1073/pnas.1815060116

Misios, S., Mitchell, D. M., Gray, L. J., Tourpali, K., Matthes, K., Hood, L., et al. (2016). Solar signals in CMIP-5 simulations: effects of atmosphere–ocean coupling. *Quarterly Journal of the Royal Meteorological Society*, *142*(695), 928–941. https://doi.org/10.1002/qj.2695

Mitchell, D. M., Misios, S., Gray, L. J., Tourpali, K., Matthes, K., Hood, L., et al. (2015). Solar signals in CMIP-5 simulations: The stratospheric pathway. *Quarterly Journal of the Royal Meteorological Society*, *141*(691), 2390–2403. https://doi.org/10.1002/qj.2530

Paek, H., Yu, J. Y., & Qian, C. (2017). Why were the 2015/2016 and 1997/1998 extreme El Niños different? *Geophysical Research Letters*, *44*(4), 1848–1856. https://doi.org/10.1002/2016GL071515

Pascolini-Campbell, M., Zanchettin, D., Bothe, O., Timmreck, C., Matei, D., Jungclaus, J. H., & Graf, H. F. (2015). Toward a record of Central Pacific El Niño events since 1880. *Theoretical and Applied Climatology*, *119*(1–2), 379–389. https://doi.org/10.1007/s00704-014-1114-2

Ratnam, M. V., Rao, N. V., Vedavathi, C., Murthy, B. K., & Rao, S. V. B. (2014). Diurnal tide in the low-latitude troposphere and stratosphere: Long-term trends and role of the extended solar minimum. *Journal of Atmospheric and Solar-Terrestrial Physics*, *121*, 168–176. https://doi.org/10.1016/j.jastp.2014.06.004

Roy, I. (2014). The role of the Sun in atmosphere–ocean coupling. *International Journal of Climatology*, *34*(3), 655–677. https://doi.org/10.1002/joc.3713

Seager, R., Harnik, N., Robinson, W. A., Kushnir, Y., Ting, M., Huang, H. P., & Velez, J. (2005). Mechanisms of ENSO-forcing of hemispherically symmetric precipitation variability. *Quarterly Journal of the Royal Meteorological Society*, *131*(608), 1501–1527. https://doi.org/10.1256/qj.04.96

Shindell, D. T., Faluvegi, G., & Schmidt, G. A. (2020). Influences of solar forcing at ultraviolet and longer wavelengths on climate. *Journal of Geophysical Research: Atmosphere*, *125*(7). e2019JD031640. https://doi.org/10.1029/2019JD031640

Sun, F., & Yu, J. Y. (2009). A 10-15year Modulation Cycle of ENSO Intensity. *Journal of Climate*, *22*, 1718–1735. https://doi.org/10.1175/2008JCLI2285.1

Thiéblemont, R., Matthes, K., Omrani, N. E., Kodera, K., & Hansen, F. (2015). Solar forcing synchronizes decadal North Atlantic climate variability. *Nature Communications*, *6*(1), 1–8. https://doi.org/10.1038/ncomms9268

Van Loon, H., Meehl, G. A., & Shea, D. J. (2007). Coupled air-sea response to solar forcing in the Pacific region during northern winter. *Journal of Geophysical Research*, *112*(D2). https://doi.org/10.1029/2006JD007378

Vimont, D. J., Wallace, J. M., & Battisti, D. S. (2003). The seasonal footprinting mechanism in the Pacific: Implications for ENSO. *Journal of Climate*, *16*(16), 2668–2675. https://doi.org/10.1175/1520-0442%282003%29016<2668%3ATSFMIT>2.0.CO;2

Wang, C. (2002). Atmospheric circulation cells associated with the El Niño–Southern Oscillation. *Journal of Climate*, *15*(4), 399–419. https://doi.org/10.1175/1520-0442(2002)015<0399:ACCAWT>2.0.CO;2

Xie, S. P., & Philander, S. G. H. (1994). A coupled ocean-atmosphere model of relevance to the ITCZ in the eastern Pacific. *Tellus*, *46*(4), 340–350. https://doi.org/10.1034/j.1600-0870.1994.t01-1-00001.x

Yu, J. Y., & Fang, S. W. (2018). The distinct contributions of the seasonal footprinting and charged-discharged mechanisms to ENSO complexity. *Geophysical Research Letters*, *45*(13), 6611–6618. https://doi.org/10.1029/2018GL077664

Yu, J. Y., & Kao, H. Y. (2007). Decadal changes of ENSO persistence barrier in SST and ocean heat content indices: 1958–2001. *Journal of Geophysical Research*, *112*, D13106. https://doi.org/10.1029/2006JD007715

Yu, J. Y., Kao, H. Y., & Lee, T. (2010). Subtropics-related interannual sea surface temperature variability in the equatorial central Pacific. *Journal of Climate*, *23*(11), 2869–2884. https://doi.org/10.1175/2010JCLI3171.1

Yu, J. Y., Kao, H. Y., Lee, T., & Kim, S. T. (2011). Subsurface ocean temperature indices for Central-Pacific and Eastern-Pacific types of El Niño and La Niña events. *Theoretical and Applied Climatology*, *103*(3–4), 337–344. https://doi.org/10.1007/s00704-010-0307-6

Yu, J. Y., Kao, P. K., Paek, H., Hsu, H. H., Hung, C. W., Lu, M. M., et al. (2015). Linking emergence of the Central-Pacific El Niño to the Atlantic Multi-decadal Oscillation. *Journal of Climate*, *28*(2), 651–662. https://doi.org/10.1175/JCLI-D-14-00347.1

Yu, J. Y., & Kim, S. T. (2013). Identifying the types of major El Niño events since 1870. *International Journal of Climatology*, *33*(8), 2105–2112. https://doi.org/10.1002/joc.3575

Yu, J. Y., Lu, M. M., & Kim, S. T. (2012). A change in the relationship between tropical central Pacific SST variability and the extratropical atmosphere around 1990. *Environmental Research Letters*, *7*(3), 034025. https://doi.org/10.1088/1748-9326/7/3/034025

Yu, J.-Y., Wang, X., Yang, S., Paek, H., & Chen, M. (2017). *Changing El Niño–Southern Oscillation and associated climate extremes, book chapter in climate extremes: Patterns and mechanisms*. In S. Y. S. Wang, J. H. Yoon, C. C. Funk, & R. R. Gillies (Eds.), Geophysical Monograph Series (Vol. *226*, pp. 3–38). Washington, DC: American Geophysical Union.

The footprint of the 11-year solar cycle in Northeastern Pacific SSTs

and its influence on the Central Pacific El Niño

Yong-Fu Lin[1], Jin-Yi Yu[1], Chau-Ron Wu[2], and Fei Zheng[3]

[1]Department of Earth System Science, University of California, Irvine, CA, USA

[2]Department of Earth Sciences, National Taiwan Normal University, Taiwan

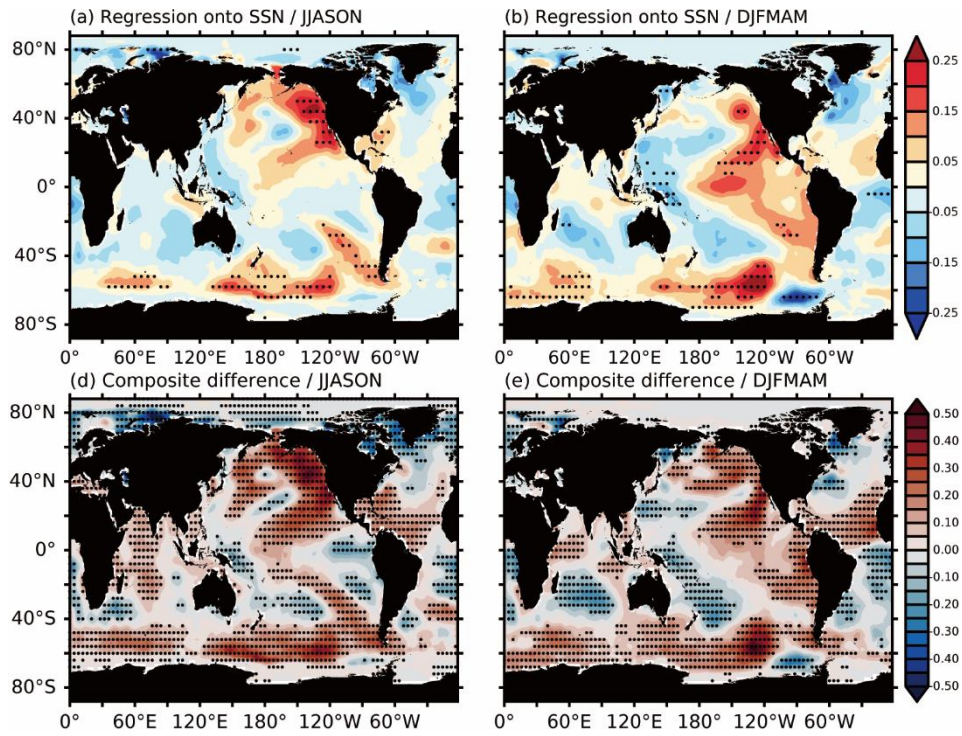[3]International Center for Climate and Environment Science (ICCES), Institute of Atmospheric Physics, Chinese Academy of Sciences, Beijing 100029, China

Contents of this file

1

Figure S1. (a) Regression of JJASON SST anomalies onto the yearly SSN (ºC/100*SSN) at 0-year lag during 1900-2018. (b) Same as (a) but for DJFMAM. (c) The difference in composite JJASON SST anomalies (unit in ºC) between active and inactive solar periods during 1900-2018. (d) same as (c) but for DJFMAM. Stippled areas indicate significance at the 95% confidence level determined using a Student's t-test.

.

Figure S2. (a) Regression of JJASON SST anomalies onto the yearly SSN (°C/100*SSN) at 0-year lag during 1900-2018. (b) Same as (a) but for DJFMAM. (c) The difference in composite JJASON SST anomalies (unit in °C) between active and inactive solar periods during 1900-2018. (d) same as (c) but for DJFMAM. Stippled areas indicate significance at the 95% confidence level determined using Student's t-test. All SST anomalies were 7-year low-pass filtered. A Least Squares Lanzcos filter was used for the filtering.

3
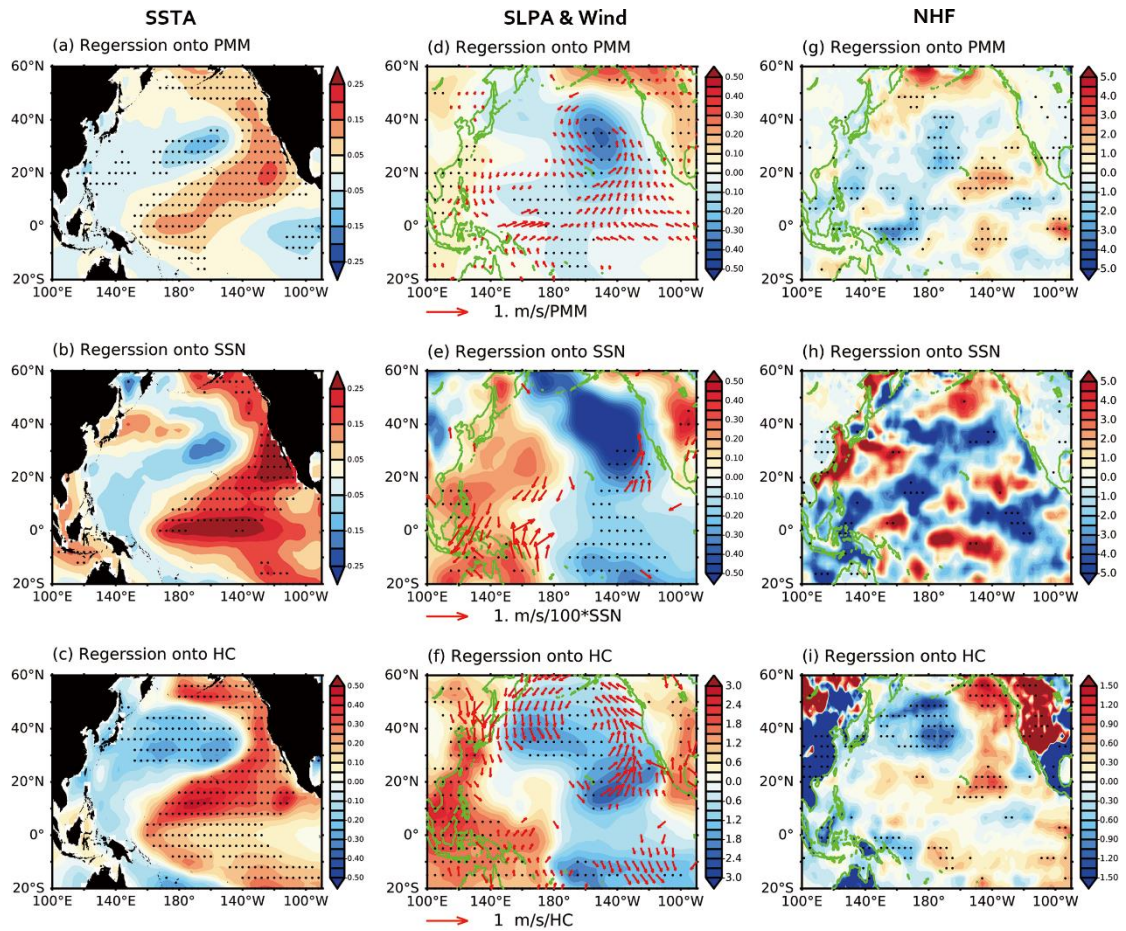
Figure S3. Regression of DJFMAM anomalies in SST (ºC) with respect to the DJFMAM PMM index (a), and yearly SSN (b), during 1948-2018. (c) Regression of the 13-month running mean of SST anomalies onto the 13-month running mean of the NE Pacific HC index (multiplied by -1). (d-f) same as (a-c), but for anomalies in SLP (hPa) and 1000 hPa wind. (g-i) same as (a-c), but for anomalies in net heat flux (W/m^2). In (d-f), only vectors at the 95% confidence level or higher are shown. Stippled areas in each figure indicate significance at the 95% confidence level determined using a Student's t-test.

4
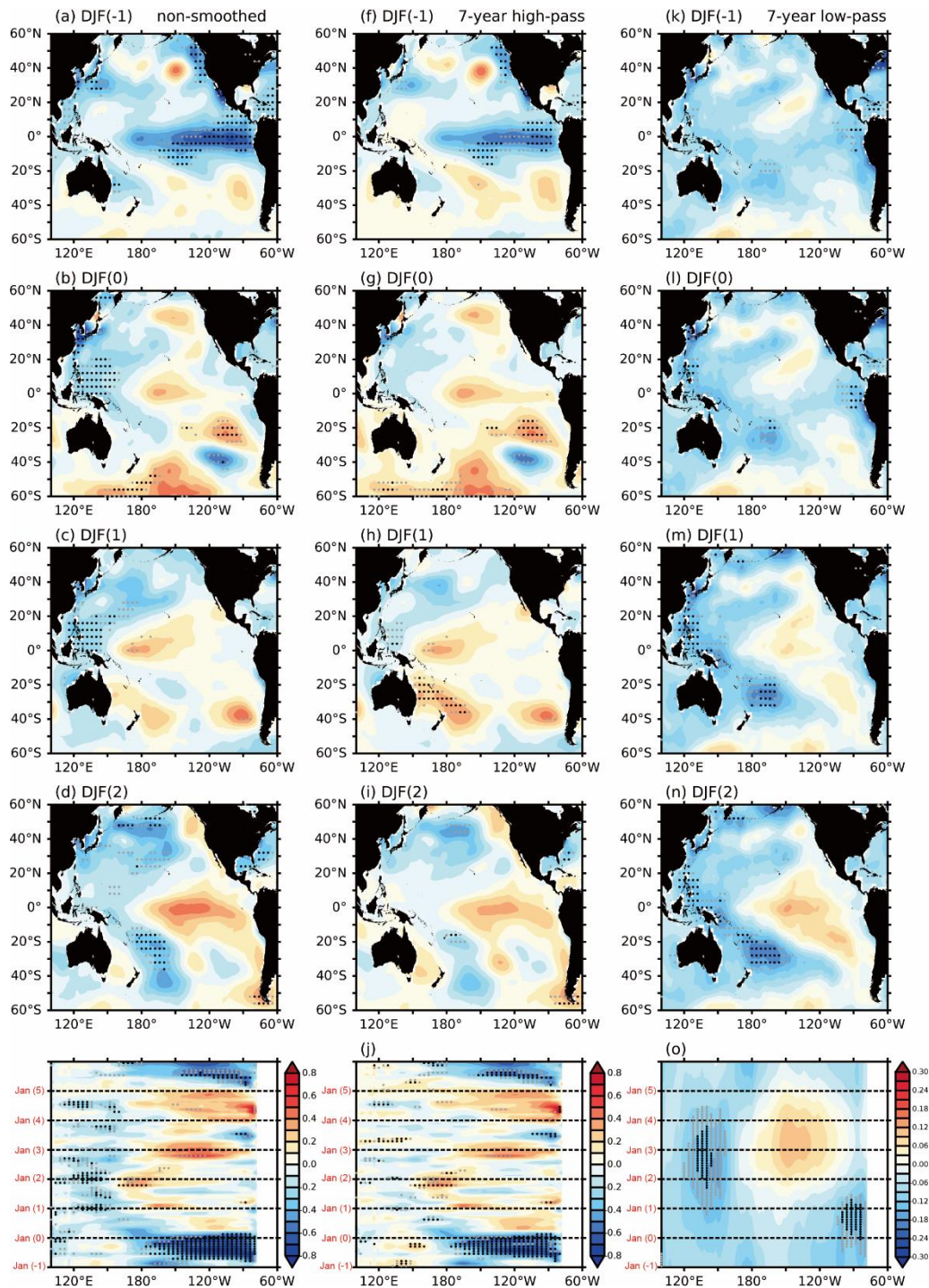
Figure S4. SSTA (unite in °C) composited from the 12 first-peak years of the solar cycle (1883, 1893, 1905, 1917, 1928, 1937, 1947, 1957, 1968, 1979, 1989, 2000; following Meehl and Arblaster, 2009) during (a) the DJF before the peak year (DJF -1), (b) the DJF of the peak year (DJF 0), (c) the 1st DJF after the peak year (DJF 1), (d) the 2nd DJF after the peak year (DJF 2). (e) Evolution of the composite monthly SSTA along the equatorial (5°S-5°N) Pacific from one year before to five years after the first-peak year and calculated with the original SST anomalies. (f-j) same as (a-e) but calculated using the 7-year high-pass filtered SSTA. (k-o) same as (a-e) but calculated using the 7-year low-pass filtered SSTA. The Least Squares Lanzcos filter was used for the filtering. Gray (black) stipples indicate areas where the composites are statistically

5

61   significance at the 90% (95%) confidence level determined using a Student's t-test.

62
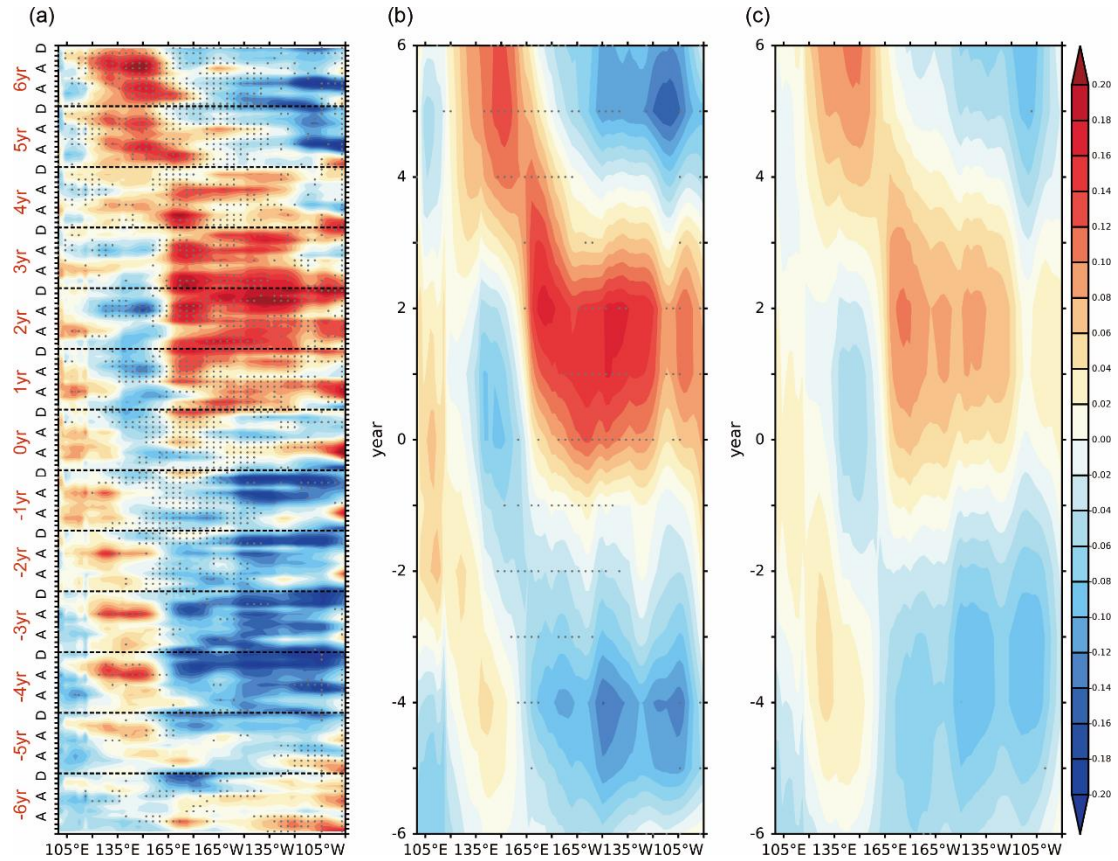
Figure S5. (a) Lagged regressions of monthly SSTA along the equator (5ºS-5ºN) Pacific, unit in ºC/100*SSN) onto the yearly SSN during 1900-2018. (b) Same as (a) but calculated with DJFMAM SSTA. (c) Same as (a) but calculated with the 7-year low-pass filtered DJFMAM SSTA. Gray stipples indicate areas where the regressions are statistically significance at the 95% confidence level determined using a Student's t-test.

73 **TABLE S1. CP La Niña and El Niño events during 1900-2016**

ENSO type	events
CP El Niño (Yu and Kim, 2013; Paek and Yu et al., 2017)	1904/05, 1914/15, 1940/41, 1941/42, 1957/58, 1963/64, 1965/66, 1968/69, 1969/70, 1977/78, 1987/88, 1991/92, 1994/95, 2002/03, 2004/05, 2009/2010
CP La Niña (Ding et al., 2017)	1903/04, 1909/10, 1910/11, 1924/25, 1933/34, 1942/43, 1949/50, 1950/51, 1970/71, 1973/74, 1975/76, 1988/89, 1998/99, 1999/2000, 2000/01, 2007/08, 2008/09, 2010/11, 2011/12

74

75